GPCR and G protein mobility in D. discoideum : a single molecule study

Hemert, F. van

Chapter 2

Mobility of G proteins is heterogeneous and polarized during chemotaxis

The interaction of G-protein-coupled receptors with G proteins is a key event in transmembrane signal transduction leading to vital decision-taking of the cell. Here we applied single-molecule epifluorescence microscopy to study the mobility of both the G$\beta\gamma$ and the Gα2 subunits of the G protein heterotrimer in comparison to the cAMP-receptor responsible for chemotactic signaling in *Dictyostelium discoideum*. Our experimental results suggest that $\sim$30% of the G protein heterotrimers exist in receptor pre-coupled complexes. Upon stimulation in a chemotactic gradient this complex dissociates, subsequently leading to a linear diffusion/collision amplification of the external signal. The further observation of partial immobilization and confinement of G$\beta\gamma$ in an agonist, F-actin and Gα2-dependent fashion led to the hypothesis of functional nanometric domains in the plasma membrane that locally restrict the activation signal and in turn lead to faithful and efficient chemotactic signaling.

2.1 Introduction

G protein mediated signaling is a widely used mechanism for transmembrane signal transduction. It entails a seven-transmembrane receptor, the G protein coupled receptor (GPCR), and a heterotrimeric G protein consisting of a Gα and a heterodimeric G$\beta\gamma$ subunit. Compared to other transmembrane signaling systems, the complex, modular mechanics of G protein linked signaling allows for divergence, convergence and regulation to take place at the level of the GPCR/G protein complex by modulation of their interaction [97]. Mammalian genomes generally encode for > 1000 GPCRs the majority of which does not have a known ligand. Although the atomic structure of three GPCRs have been resolved so-far [69, 77, 43] a mechanism for how ligand induced conformational changes lead to G protein activation is still unknown. Even the simple quest of whether GPCRs and G proteins can exist together in a stable complex or interact dynamically has been solved for only one system [67]. In the dogmatic view the ligand-based activation of the GPCR promotes the exchange of guanosine diphosphate (GDP) for guanosine triphosphate (GTP) in the Gα subunit which subsequently dissociates from the complex allowing both Gα and G$\beta\gamma$ to engage in downstream signaling. Hydrolysis of GTP to GDP in the Gα subunit, either autocatalytically or by effector proteins, leads to re-association of the GPCR/G$\alpha\beta\gamma$ complex.

An intriguing system in which GPCR signaling leads to a dramatic change in cellular behavior is that of eukaryotic chemotaxis. Chemotaxis controls e.g. the developmental cycle in the social amoeba *Dictyostelium discoideum*. Generally, chemotaxis is interpreted as a three-stage process starting with gradient sensing followed by cellular polarization, ultimately resulting in directional movement. *D. discoideum* cells secrete cyclic adenosine mono-phosphate (cAMP) that acts as a chemoattractant leading to cell aggregation. Aggregation is achieved by a chemotactic process being initiated by activation of the cAMP receptor 1 (cAR1) which in turn activates a G protein heterotrimer, consisting of a Gα2 and a G$\beta\gamma$ subunit [49]. Sequencing of the *D. discoideum* genome showed that there are two Gβ and a single Gγ subunit type in *D. discoideum* [60, 102, 20].Consequently these G$\beta\gamma$ heterodimers participates in all GPCR triggered responses. Receptor-mediated activation of heterotrimeric G

protein complexes was visualized in *D. discoideum* using Förster Resonance Energy Transfer (FRET) between the Gα2 and Gβ subunits, fused to cyan and yellow fluorescent proteins respectively [44]. These FRET experiments demonstrated that G protein heterotrimers are stable in the absence of agonist and rapidly dissociate upon addition of cAMP. Recently the FRET experiments were complemented with Fluorescence Recovery After Photobleaching (FRAP) data. A new model for G protein signaling was suggested in which the Gα2 increases the time it spends on the membrane or in a cAR1-bound state and the activated G$\beta\gamma$ subunit dissociates into the cytosol. Both processes will lead to a cycling of the G protein heterotrimer between the membrane-bound and a free cytosolic state [22].

Although many molecular details of the pathways are known, a direct connection between gradient sensing and the movement machinery is still to be discovered. At this moment there are several pathways known to act in parallel downstream of G protein activation that mediate the final chemotactic response. The most thoroughly studied pathway involves PI3-kinase (PI3K) and its antagonist, a PI3-phosphatase (PTEN). The coördinated action of both leads to local accumulation of PI(3,4,5)P_3 in the leading edge of the crawling cells [40, 30]. Recently, additional pathways have been discovered to act in parallel; the phospholipase A2 (PLA2) pathway [11] and the TorC2 pathway [48].

In cells placed in a gradient of cAMP, the pathways downstream of G protein signaling trigger actin polymerization selectively in the cell's leading edge, whereas actin polymerization occurs globally upon uniform cAMP stimulation [12]. Unlike the highly polarized localization in actin polymerization and the preceding highly polar translocation of a variety of intracellular signaling molecules like PI(3,4,5)P_3 and PI(4,5)P_2, receptor localization is fully homogeneous. The G$\beta\gamma$ subunit of the G protein is localized in a shallow anterior-posterior gradient, however at a level of polarization impossible to restrict signaling to the leading edge [46]. Recent studies [17] revealed however a spatially restricted increase of receptor mobility in the leading edge of *D. discoideum* cells when exposed to a stable cAMP gradient. Those data suggested an asymmetry in the activation level of the receptor-G protein pathway with a predicted linear amplification of the local activation level of the G proteins.

Here we set out to address this prediction. We analyzed Gα2 and G$\beta\gamma$ mobility

in the absence of agonist, upon uniform cAMP stimulation and in a cAMP gradient using single-molecule epifluorescence microscopy [81]. We found that Gα2 and Gβγ occur as a smaller (∼30%) receptor-precoupled fraction, and a larger (∼70%) receptor-uncoupled fraction. Upon global stimulation with cAMP the receptor-coupled fraction disappeared. In terms of the receptor those occupation numbers correspond to about 50% of all available receptors. The activated Gβγ molecules immobilize in an F-actin dependent manner. Concurrently, the formation of F-actin-dependent domains of size ∼600 nm was observed. Strikingly the dramatic changes in mobility were restricted to the leading edge of chemotaxing cells. We propose that Gβγ immobilization is caused by its incorporation into a larger signaling complex, a signalosome for which F-actin functions as a scaffold. Such a mechanism would lead to stabilization of pseudopods and the formation of a persistent leading edge by means of a direct F-actin - G protein feedback loop.

2.2 Materials and methods

2.2.1 Cell culturing and transformation

The axenically growing *D. discoideum* strain Ax2 [93] was used in this study and referred to as wild-type (wt), to discriminate from other genetic backgrounds that were used. The wt, $g\beta^-$ (LW5, [60]), $g\alpha2^-$ (myc2, [13]) and *car1*$^-$ [9] cells were transformed by electroporation with a plasmid, encoding the Gβ-YFP fusion protein. The same procedure was followed for wt, $g\alpha2^-$ and *car1*$^-$ cells with the plasmid encoding for the Gα2-YFP fusion protein. G418 (Geneticin, Invitrogen) was used to select for successfully transformed *D. discoideum*. Cells were grown as a monolayer on plastic dishes in axenic culture medium, HL5-C (Formedium), containing 10 µg/ml penicillin/streptomycin (1:1) (Invitrogen) and 20 µg/ml G418, at 22 °C.

2.2.2 Cell preparation for measurements

To assess chemotactic competence, *D. discoideum* cells from axenic exponentially growing cultures were cultured in a plastic dish overnight in low fluorescence medium (Formedium). The physiological state of the cells treated in this way was compara-

ble to 1-2 hr starved cells. After that the cells were detached from the plate, washed three times with developmental buffer [24], centrifuged for 3 min at 400×g RCF, and resuspended in 5 ml developmental buffer at a concentration of $\sim 10^7$cells/ml in a 100 ml Erlenmeyer flask. After 1 hr of shaking at 100 rpm the cells were pulsed with a peristaltic pump (Gilson, Minipulse 2) with 150 nM cAMP at 6 min intervals, for 4 hr for the transformants in wt, and overnight for the transformants in knock-out backgrounds [21]. After pulsing, the cells were shaken for an additional 30 min and finally diluted in developmental buffer to a concentration of 10^6 cells/ml. Cells were transferred into 2-well chambered cover glasses (1.5 Borosilicate Sterile, Lab Tek II) where they were allowed to adhere.

2.2.3 Developmental test

Gα2-YFP/$g\alpha 2^-$ and Gβ-YFP/$g\beta^-$ transformants, as well as $g\alpha 2^-$ and $g\beta^-$ cells were pulsed overnight with 150 nM cAMP per pulse and subsequently plated on non-nutrient 1.5% agar plates at a concentration of 3-4 $\cdot$ 10^7 cells/cm^2. After 24 hr the developmental state was assessed.

2.2.4 Global cAMP stimulation assay

The developmental buffer, covering the developed cells in the chambered cover-glasses was supplemented with cAMP to a final concentration of 10 µM. Experiments were performed within 20 min after addition of cAMP.

2.2.5 Chemotaxis micropipette assay

Cells were placed at a distance of $\sim$75 µm from the opening (r = 0.25 µm) of a pipette (Eppendorf femtotip) filled with 10 µM cAMP. The internal pressure in the pipette was set to 40 KPa by means of a FemtoJet injector (Eppendorf). This setup created a stable, shallow gradient estimated at 0.4 nM/µm cAMP over the cell body at a mid concentration of $\sim$60 nM. The gradient caused polarization of the developed *D. discoideum* cells towards the micropipette tip. The region-of-interest was set to the leading and trailing edge (20% of the cell body) of a polarized cell, respectively.

2.2.6 Latrunculin A treatment

The developmental buffer, covering the developed cells in the chambered coverglasses was supplemented with 0.5 µM latrunculin A. After 10 min, single-molecule measurements were performed for 10 min. To observe the effect of latrunculin A on the cell's response to cAMP, 10 min after addition of the latrunculin A, cAMP was added to the buffer at final concentration of 10 µM, measurements were taken within 10 min of cAMP addition [28].

2.2.7 Single molecule microscopy

The experimental setup for single-molecule imaging has been described in detail previously [81]. The samples were mounted onto an inverted microscope (Axiovert100, Zeiss) equipped with a 100× objective (NA=1.4, Zeiss). The region-of-interest was set to 50 × 50 pixels. The apparent pixelsize was 220 nm. Measurements were performed by illumination of the samples for 5 ms at 514 nm (Argon-ion laser, Spectra Physics) at an intensity of 2 kW/cm^2. The cells were photobleached for a period of 2-5 s and sequences of 500 images with a timelag of 50 ms were taken. Use of an appropriate filter combination (Chroma) permitted the detection of the fluorescence signal on a liquid nitrogen-cooled CCD-camera (Princeton Instruments). The setup allowed imaging of individual fluorophores at a signal-to-background-noise ratio of $\sim$30 leading to a positional accuracy of σ_0 = $\sim$40nm.

2.2.8 Estimation of the expression level of Gα2-YFP and Gβ-YFP

The expression level of Gα2-YFP in $g\alpha2^-$, and Gβ-YFP in $g\beta^-$ cells was calculated in the following manner. The image of a single fluorescent molecule was given by an intensity distribution characterized by a full-width-at-half-maximum of w_0 = 1.7 pxl = 0.37 µm. The average signal for a single YFP molecule was S_1 = 220 cnts when illuminated with 2 kW/cm^2 for 5 ms at 514 nm [36]. The fluorescence of Gβ-YFP at the apical membrane at identical conditions was $S_{G\beta}$ = 4300 cnts/pxl, and for Gα2-YFP $S_{G\alpha2}$ = 4000 cnts/pxl. The surface of the membrane for a whole cell (approximated by a spheroid with a short axis of r_1= 5 µm and long axis r_2= 10 µm) is about 540 µm^2. The fluorescence data were used in the estimation of the

expression level yielding $S_{G\beta}$ / $S_1 \cdot A/{w_0}^2$ = $7.7 \cdot 10^4$ Gβ-YFP and $7.2 \cdot 10^4$ Gα2-YFP molecules per cell. A similar estimation has been done for the receptor yielding $4 \cdot 10^4$ cAR1 per cell [17].

2.2.9 Particle image correlation spectroscopy (PICS)

The reconstruction of trajectories from molecule positions is severely hampered by blinking and photobleaching of eYFP [36]. Therefore we used an alternative analysis method, particle-image-correlation-spectroscopy (PICS), described in detail elsewhere [83]. In short, the cross-correlation between single-molecule positions at two different time lags is calculated. Subsequently, the linear contribution from uncorrelated molecules in close proximity is subtracted. This results in the cumulative distribution function $cdf(r^2, t_{lag})$ which yields the distribution of squared jump widths between within the given time lag t_{lag}. For each time lag $cdf(r^2, t_{lag})$ is fitted to a two fraction model (eq.2.2).

2.2.10 Analysis of the cumulative probability functions

From the jump width distributions the diffusion characteristics of all molecules is extracted. Given that the population of particles is homogeneous, the diffusion equation is solved for $cdf(r^2, t_{lag})$ given by:

$$cdf(r^2, t_{lag}) = \alpha \cdot \exp\left(-\frac{r^2}{MSD_1}\right) \tag{2.1}$$

where $MSD(t_{lag})$ is the mean square displacement at time lag t_{lag}. Given the exponential distribution in r^2 data are represented on $\log(r^2)$-scale. Our experimental data could not be fitted with this one fraction model, however (fig.2.2A). Therefore the data were fit to a two-fraction model described by:

$$cdf(r^2, t_{lag}) = 1 - \left(\alpha \cdot \exp\left(-\frac{r^2}{MSD_1}\right) + (1-\alpha)\exp\left(-\frac{r^2}{MSD_2}\right)\right) \tag{2.2}$$

where $MSD_1(t_{lag})$ is the characteristic mean squared displacement for the fast fraction of size α, and $MSD_2(t_{lag})$ the characteristic mean squared displacement for

the slow fraction of size 1-α. The bi-exponential fit properly describes the experimental results (fig.2.2A). This showed that there are two fractions of Gβ-YFP and of Gα2-YFP molecules that differ in their mobility on the membrane. Molecules were defined immobile when their MSD for the largest time lag (0.4 sec) was smaller than twice the positional accuracy. Together with equation 2.3 this leads to an upper estimate for their diffusion constant of $D_{immobile} < 0.001\ \mu m^2/s$.

2.3 Results

2.3.1 Heterogeneity in the mobility of Gα2-YFP and Gβ-YFP in the absence of agonist

D. discoideum cells were transformed stably with Gα2-YFP or Gβ-YFP constructs to analyze the mobility of individual Gα2 and G$\beta\gamma$ molecules, respectively. The fluorescent fusion proteins were functional as they rescued the developmental and chemotactic defects of $g\alpha 2^-$ and $g\beta^-$ cells. In contrast to $g\alpha 2^-$ and $g\beta^-$ cells that both are fully deficient in cAMP-induced responses, the Gα2-YFP/$g\alpha 2^-$ and Gβ-YFP/$g\beta^-$ transformants faithfully crawl towards a cAMP source and rescue the developmental cycle started upon starvation [46, 44].

Single-molecule microscopy, a combination of regular wide-field microscopy with laser excitation and ultra-sensitive CCD camera detection [81], was used to observe the diffusion of Gα2-YFP and Gβ-YFP on the apical cellular membrane of *D. discoideum*. Measurements on the apical membrane eliminate any potential influence of the substrate surface on mobility. Fluorescence images were taken consecutively for up to 500 images per sequence at an imaging rate of 20 Hz. Diffraction-limited fluorescent signals with signal strengths comparable to that reported for individual monomeric YFP molecules [36] were observed and followed over time (fig.2.1B&C). Given the signal-to-noise ratio achieved the position of each molecule was determined to an accuracy of $\sim$40 nm. Statistical significance of all results was assured by the analysis of > 40 cells for each experimental condition. In total our analysis is based on 1-4 $\cdot$ 10^4 observed molecules per condition.

Particle image correlation spectroscopy (PICS) [83] was subsequently applied to construct the cumulative probability (cumulative density function, cdf) of the squared

displacements for time-lags of 0.05-0.4 sec (fig.2.1D, fig.2.2A&B). To our surprise it became obvious for all cdfs that G protein mobility was not homogeneous and was best described by a two-fraction model (fig.2.2A) which, after fitting, yielded a fraction size and two mean squared displacements per time-lag (see section 2.2). The result of a final analysis is shown in figure 2.2C&D for the fast and slow fraction of Gβ-YFP in non-stimulated aggregation competent cells, respectively (supplemental fig.2.8 for results on Gα2-YFP). For both fractions the mean squared displacement, MSD, increased linearly with time-lag, indicative of free Brownian motion of the proteins within the membrane characterized by diffusion constant D,

$$MSD(t_{lag}) = 4Dt_{lag} + s_0 \tag{2.3}$$

where the offset, s_0, accounts for the limited positional accuracy, σ, in the experiment ($s_0 = 4\sigma^2 = 0.0064$ μm^2 with σ = 40 nm). Because the Gγ subunit has been shown to be essential for the membrane localization of Gβ [102] we assume, in what follows, that Gβγ is in heterodimeric form and all information obtained for Gβ reflects in an identical manner the behavior of Gγ. For Gβγ-YFP in unstimulated cells the fast fraction was characterized by a diffusion constant $D_1 = 0.15 \pm 0.01$ μm^2/s, and the slow fraction, consisting of $32 \pm 3\%$ of all molecules, was characterized by $D_2 = 0.011 \pm 0.001$ μm^2/s. For the membrane-bound Gα2-YFP in unstimulated cells the respective diffusion constants of the fast and the slow fraction were $D_1 = 0.14 \pm 0.01$ μm^2/s and $D_2 = 0.015 \pm 0.001$ μm^2/s, with the slow fraction constituting $32 \pm 4\%$ of the total pool of molecules (supplemental fig.2.8). Identical results for the mobility and fraction size of Gα2 and Gβγ were obtained in $g\alpha 2^-$ and $g\beta^-$ cells that expressed Gα2-YFP and Gβ-YFP respectively at endogenous levels (supplemental fig.2.9). The latter findings proved that the predominant fast fraction was not an artifact caused by the over-expression of the constructs in a wt background.

2.3.2 Mobility suggests the existence of a receptor/G protein precoupled complex in the absence of agonist

The strong similarity of the diffusion constants of both fractions for Gα2 and Gβγ further suggests that all membrane-bound G proteins in unstimulated cells were Gα2βγ

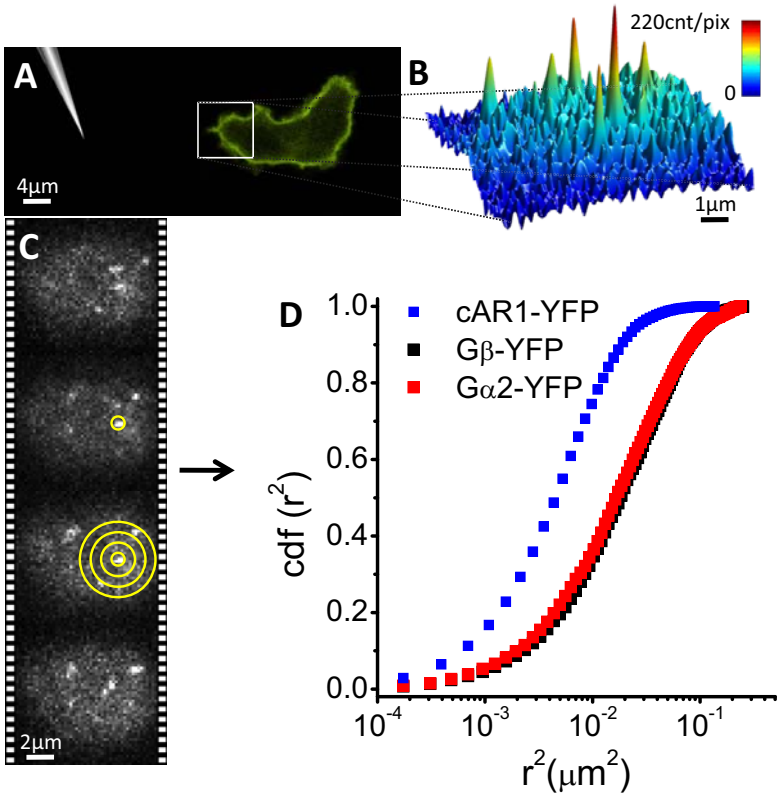

Figure 2.1: Experimental setup. **(A)** A micropipette containing 10 µM cAMP created a stable concentration gradient around its opening. *D. discoideum* cells in the vicinity of the pipette opening polarized within minutes and moved up the cAMP concentration gradient. The anterior and posterior of a cell were defined as the part closest and farthest away from the pipette, respectively. **(B)** A 514 nm laser beam was focused on the apical cell membrane where signals originating from individual Gβ-YFP or Gα2-YFP proteins were observed with a signal-to-noise ration of ∼30. **(C)** Single-molecule positions were determined to an accuracy of ∼40 nm by fitting to a 2D-Gaussian profile. Image-stacks were analyzed using PICS (see section 2.2.9), yielding the cumulative density functions of squared displacements ($cdf(r^2)$) for each time lag. **(D)** Cdfs at time lag of 50 ms are compared for cAR1-YFP (blue), Gβ-YFP (black) and Gα2-YFP (red).

heterotrimers. It is tempting to associate the slow mobility fractions of Gα2 and Gβγ to a receptor/G protein precoupled complex. The G protein diffusion constants (D_2= 0.015 μm^2/s for Gα2 and D_2= 0.011 μm^2/s for Gβγ) were similar to that found for the fast fraction of the receptor cAR1 ($MSD_{(44ms)}$ = 0.034 μm^2 [17]; D = 0.015 μm^2/s, see chapter 3). On the other hand, the diffusion constants of the fast fractions of the G protein subunits in unstimulated, aggregation competent cells were one order of magnitude higher than that found for cAR1, demonstrating that the fast fraction cannot be associated with a receptor-precoupled complex.

The association of the slow G protein fractions with a receptor/G protein precoupled complex was further supported by the analysis of Gβ-YFP mobility in *car1*$^-$and in $g\alpha2^-$ cells (fig.2.3). Both, Gβ-YFP/*car1*$^-$and Gβ-YFP/$g\alpha2^-$ cells were fully deficient in chemotactic signaling and unable to aggregate. For both cell types mobility was best described by a two-fraction model, with decreased slow fraction size of 18 ± 3% and 27 ± 4% for Gβ-YFP/*car1*$^-$ and Gβ-YFP/$g\alpha2^-$, respectively (fig.2.3A). In addition, the diffusion constants of the slow fraction of Gβ-YFP in both knock-out cells was found to be D_2 = 0.020 ± 0.001 μm^2/s in $g\alpha2^-$ and D_2 = 0.023 ± 0.001 μ^2/s in *car1*$^-$, respectively (fig.2.3B, left), higher as compared to the diffusion constants in wild-type (wt) cells, and in particular the diffusion constant of cAR1. In comparison, the mobility of the fast fractions, D_1 = 0.16 ± 0.01 μm^2/s in $g\alpha2^-$ and D_1 = 0.19 ± 0.01 μm^2/s in *car1*$^-$, were found unchanged as compared to wt cells (fig.2.3C, left). Within experimental uncertainty Gα2 mobility was unchanged in *car1*$^-$ and $g\beta^-$ cells (supplemental fig.2.8B&C, left).

Additional support for our hypothesis on association of the slow fraction with a receptor/G protein precoupled complex was obtained from the estimated expression levels of all components in wt and knock-out cells. We used the membrane-localized fluorescence signal to estimate the density of Gβ-YFP and Gα2-YFP (see 2.2). Approximately $7.7 \cdot 10^4$ Gβ-YFP were expressed, which is at the lower end of the expression level of reported endogenous Gβγ molecules of 8-40 $\cdot 10^4$ molecules [46]. It was reported earlier that $4 \cdot 10^4$ receptors were expressed in wt as well as in transformed cells [34, 17], the active fraction of which, $2 \cdot 10^4$ (∼50% of $4 \cdot 10^4$ [17]) corresponds very well to the number of slow Gβγ molecules, $2.5 \cdot 10^4$ (∼32% of $7.7 \cdot 10^4$).

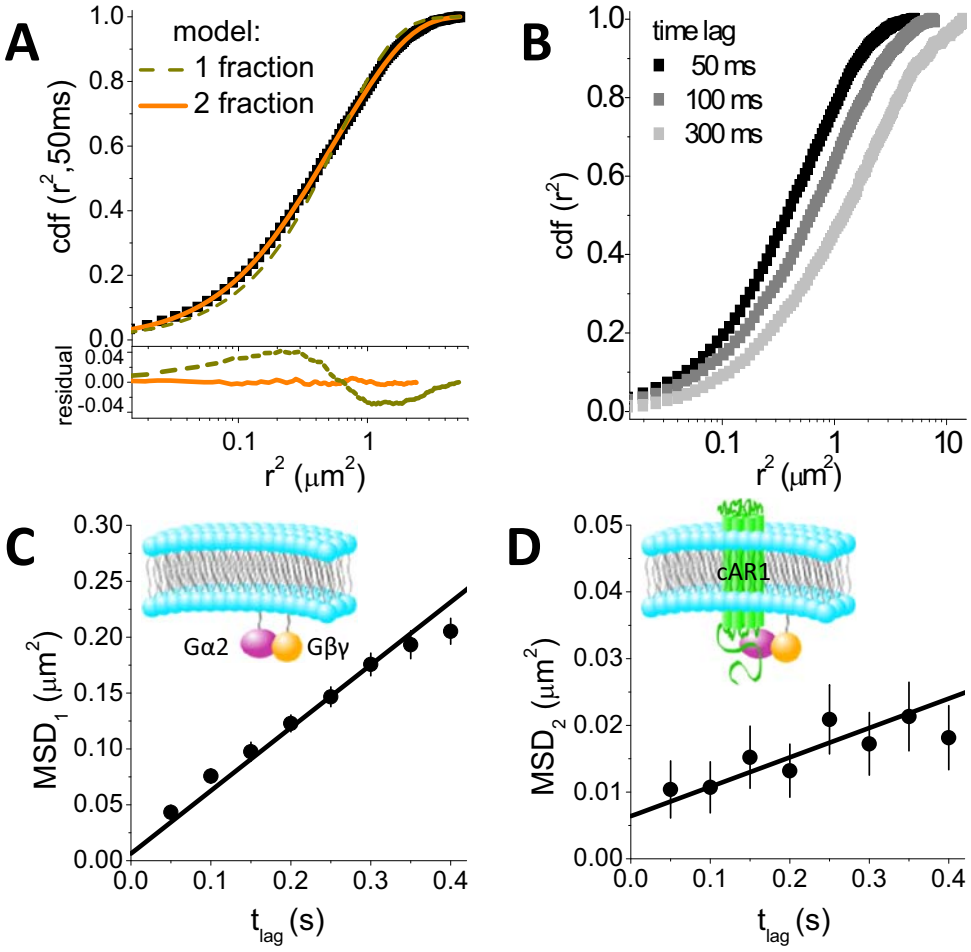
A
model:
1 fraction
2 fraction
cdf (r2,50ms)
residual
r2 (μm2)
B
time lag
50 ms
100 ms
300 ms
cdf (r2)
r2 (μm2)
C
Gα2
Gβγ
MSD1 (μm2)
tlag (s)
D
cAR1
MSD2 (μm2)
tlag (s)

Figure 2.2: Mobility of Gβ-YFP. (A) Cumulative probability distribution of the square displacements $cdf(r^2)$ of Gβ-YFP on the apical membrane of developed Gβ-YFP/wt, recorded with a time interval of 50 ms between subsequent images. Data were fitted to a two component model (eq.2.2) (orange solid line; residuals are displayed in the lower part of the figure), resulting in a fraction (α) of slow Gβ subunits, and a fraction (1-α) of fast Gβ subunits. The two fraction model describes the experimental results well in all the experimental conditions described. For comparison, a one-fraction model fit (eq.2.1) is shown (dark yellow dashed line). **(B)** Cumulative probability distributions of the square displacements on the apical membrane of developed Gβ-YFP/wt cells after 50 (black), 100 (gray), and 300 ms (light gray) time lag. As expected the data shifts with time lag towards higher squared displacements, r^2. **(C)** The characteristic mean squared displacements (MSD_1) were plotted versus time lag for the first ten time lags (50-500 ms) for the fast fraction of Gβ-YFP in wt cells. The data was fit with a free-diffusion model (eq.2.3), yielding a diffusion constant of D_1 = 0.15 $\pm$ 0.01 μm^2/s. **(D)** Mean squared displacements (MSD_2) versus time lag for the slow fraction of GβYFP in wt cells. The free-diffusion model (eq.2.3) yielded a diffusion constant of D_2 = 0.011 $\pm$ 0.001 μm^2/s. The offset at zero time lag, s_0, in (C) and (D) is given by the limited positional accuracy, $s_0 = 4\sigma^2$ = 0.0064 μm^2 with σ = 40 nm. The mobility of the slow fraction is equivalent to that of the cAMP receptor D_{cAR1} = 0.015 μm^2/s (see chapter 3).

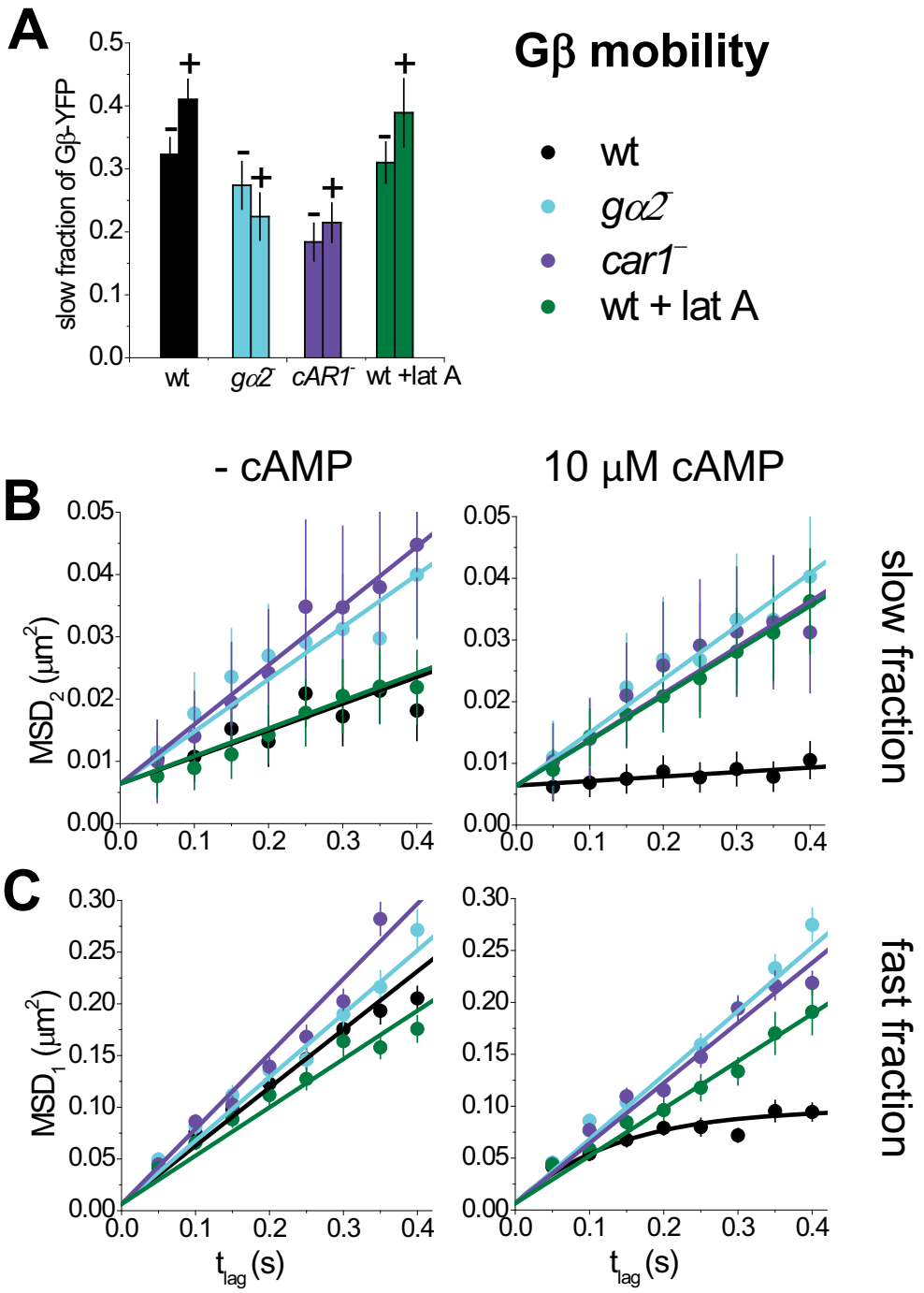
A
slow fraction of Gβ-YFP
0.0
0.1
0.2
0.3
0.4
0.5
wt
gα2-
cAR1-
wt +lat A
Gβ mobility
wt
gα2-
car1-
wt + lat A
B
- cAMP
10 µM cAMP
MSD2 (µm2)
slow fraction
C
MSD1 (µm2)
tlag (s)
fast fraction

Figure 2.3: Mobility of Gβ-YFP upon stimulation. (For the mobility of Gα2-YFP see supplemental fig.2.8) **(A)** Size of the slow fraction for Gβ-YFP in wt (black), *gα2-* (light blue), *car1*$^-$ (violet), and wt cells treated with 0.5 µM lat A (green), before and after global stimulation with 10 µM cAMP (indicated by - and +, respectively). The slowly diffusing population of Gβ-YFP in wt cells increased after cAMP stimulation. The slow fractions of Gβ-YFP in $g\alpha2^-$ and *car1*$^-$ were smaller and did not change significantly upon cAMP addition. In lat A treated cells the slow fraction was the same when compared to untreated cells. After stimulation, however, there was an increase similar to that found for cells with intact actin cytoskeleton. **(B)** MSD_2 versus time lag plot of the slow fraction of Gβ-YFP in wt (black), $g\alpha2^-$ (light blue), *car1*$^-$ (violet), and wt cells after treatment with 0.5 µM lat A (green) before (left) and after (right) stimulation with 10 µM cAMP. In wt cells the slow fraction was fully immobilized after cAMP stimulation. Gβ-YFP in $g\alpha2^-$ and *car1*$^-$ cells was diffusing nearly two times faster than Gβ-YFP in wt cells. In the knock-out strains cAMP addition did not influence the diffusion constants, suggesting that immobilization of the slow population of Gβ-YFP in wt cells was due to signaling events. Lat A treated wt cells did not show any immobilization suggesting that immobilization is caused by interaction of the Gβ subunit with F-actin structures. **(C)** MSD_1 versus time lag of the fast fraction of Gβ-YFP in wt (black), *gα2-* (light blue), *car1*$^-$ (violet), and wt cells treated with 0.5 µM lat A (green) before (left) and after (right) stimulation with 10 µM cAMP. The diffusion behavior of Gβ-YFP in wt cells changed from free (eq.2.3) to confined (eq.2.4) upon cAMP stimulation. This was not observed in lat A treated, $g\alpha2^-$, and *car1*$^-$ cells, where G protein signaling was impaired.

2.3.3 A fraction of Gβ-YFP becomes immobilized upon cAMP-induced receptor activation

To study the effect of cAMP-induced activation on Gα2 and Gβγ mobility, cells were uniformly stimulated with 10 μM cAMP. Single-molecule data were taken between 1 and 20 min after addition of cAMP (see section 2.2.4). A redistribution of the fraction sizes and mobilities was observed. The slow fraction of Gβ-YFP increased to 41 ± 3% upon stimulation (fig.2.3A), and became immobile ($D_2 \leq 0.001$ μm^2/s; fig.2.3B, right).

Neither immobilization nor change in fraction size was observed for Gα2-YFP fig.2.8. As Gα2 cycles rapidly between the membrane and the cytosol upon stimulation of cAR1 [22] this latter finding suggests that a receptor/Gα2 complex is formed prior to the full receptor/G protein heterotrimer complex.

The increase of the Gβ-YFP slow fraction and concomitant immobilization was not observed in Gβ-YFP/*car1*$^-$and Gβ-YFP/*gα2*$^-$ cells, where the slow fraction was 22 ± 4% and 21 ± 3% after stimulation, respectively (fig.2.3A and fig.2.3B right). This remaining slow fraction may be bound to other Gα subunits that are related to signaling via other G protein coupled receptors. Whereas the result on Gβ-YFP/*car1*$^-$ was predicted, the lack of Gβ-YFP response in Gβ-YFP/*gα2*$^-$ cells supports the notion that coupling to and activation by cAR1 requires Gα2. These observations together were taken as further support for the hypothesis that the slow Gα2-YFP and Gβ-YFP population reflected a receptor/G protein precoupled complex which dissociates upon ligand binding and receptor activation.

2.3.4 cAMP stimulation induces confined diffusion of fast Gα2-YFP and Gβ-YFP fractions into 600 nm membrane domains

Upon global cAMP stimulation, the fast fractions of both Gα2-YFP and Gβ-YFP changed their behavior from free diffusion (eq.2.3) to confined diffusion (fig.2.4, eq.2.4). Confined diffusion is a process in which a molecule is free to diffuse in a restricted domain surrounded by impermeable fences. The corresponding relation between MSD and timelag is:

$$MSD(t_{lag}) = \frac{l^2}{3}\left(1 - exp\left(\frac{-12D_{init}t_{lag}}{L^2}\right)\right) + s_0 \tag{2.4}$$

where D_{init} is the initial diffusion coefficient for small time-lags, and L represents the side-length of a square domain [57]. From figure 2.4B the domain size was determined to be 600 $\pm$ 100 nm for both Gα2-YFP and Gβ-YFP, and the initial diffusion constants $D_{init,1}$= 0.19 $\pm$ 0.02 and $D_{init,1}$ = 0.16 $\pm$ 0.02 $\mu m^2/s$ for the two constructs, respectively.

2.3.5 cAMP-induced membrane domains and Gβ-YFP immobilization are F-actin dependent

To determine whether there is a relation between actin polymerization, the 600 nm membrane domains, and the cAMP-induced immobilization of the G$\beta\gamma$ slow fraction, aggregation-competent Gβ-YFP/wt cells were incubated with 0.5 µM latrunculin A (lat A) for 10 min. The diffusion behavior of Gα2-YFP and Gβ-YFP was unchanged after lat A treatment in unstimulated cells (fig.2.3B&C, left; fig.2.8). However, upon global stimulation with 10 µM cAMP a significant change in the diffusion behavior was observed. The slow fraction size of Gβ-YFP increased slightly to 39 $\pm$ 5%, and the immobilization seen for untreated cells disappeared (D_2= 0.016 $\pm$ 0.001 $\mu m^2/s$; fig.2.3B, right). Further, the confinement observed in the fast fractions of Gα2-YFP and Gβ-YFP vanished and both constructs diffused freely with D_1 = 0.15 $\pm$ 0.01 $\mu m^2/s$ (fig.2.3C right; fig.2.8C). These results led us to conclude that the membrane domains observed were F-actin dependent, and that immobilization of Gβ-YFP required either a direct or an indirect interaction of Gβ-YFP with the F-actin meshwork. It should be noted however, that the increase of the slow fraction upon global cAMP stimulation was undisturbed by lat A. In contrast, the immobilization of the slow Gβ-YFP fraction was clearly regulated by F-actin and is presumably involved in maintaining cell polarity during chemotaxis.

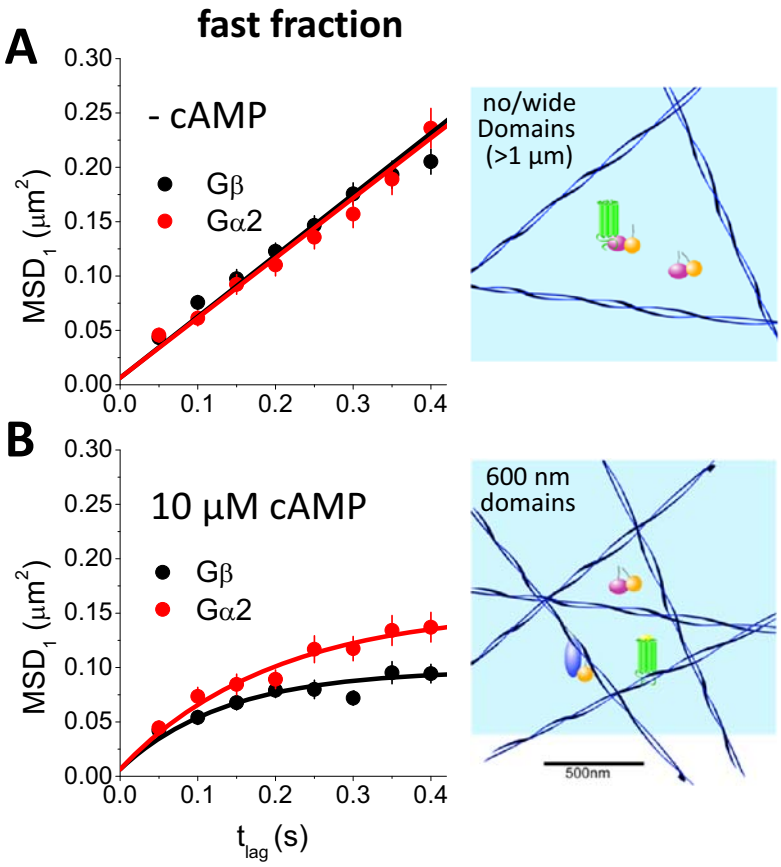

Figure 2.4: Comparison of the mobility of the fast fractions of Gβ-YFP and Gα2-YFP. The behavior of the fast Gβ-YFP (black) and Gα2-YFP (red) on the apical membrane of wt *D. discoideum* **(A)** before, and **(B)** after uniform stimulation with 10 μM cAMP changes from free to confined diffusion respectively. The formed domains have an average side length of 600 nm.

2.3.6 The increase of the slow fraction and G$\beta\gamma$ immobilization occur selectively in the leading edge

Whether the increase of the slow fraction and immobilization of Gβ-YFP upon global stimulation with 10 μM cAMP reflects a differential G protein behavior in the chemotaxis process was subsequently tested in a micropipette assay. The opening of a micropipette, filled with 10 μM cAMP, was placed at a distance of ∼75 μm from the cells generating a shallow cAMP gradient of ∼0.4 nM/μm at the cell position. After 13 min cells became highly polarized and oriented towards the micropipette (fig.2.1A). The size of the slow fraction of Gβ-YFP differed significantly when comparing leading to trailing edge and was found to be 38 ± 4% and 23 ± 3%, respectively (fig.2.5A). Strikingly we found that the diffusion constants of the slow fraction were different at the anterior as compared to the posterior: at the anterior the slow Gβ-YFP fraction was immobilized (D_2 < 0.001 $\mu m^2/s$; fig.2.5C, left) exactly as observed upon global stimulation whereas at the posterior the diffusion constant was comparable to the one found for unstimulated cells (D_2 = 0.012 ± 0.001 $\mu m^2/s$). We also found that the formation of the characteristic 600 nm domains was restricted to the anterior (fig.2.5B). All together, the behavior of G$\beta\gamma$ in the absence of agonist matches the behavior in the posterior whereas G$\beta\gamma$ behavior at the anterior matches the situation observed after global agonist stimulation. Micropipette experiments on lat A treated cells confirmed that F-actin, in part, controls G protein mobility in an activation dependent manner. As lat A pretreated cells did not evolve any morphological polarity we defined the part nearest to the micropipette as the anterior. The posterior part of the cell was defined accordingly. The difference in slow fraction size between the anterior and the posterior cell regions was found to be the same as that found in polarized cells with intact cytoskeleton (fig.2.4A, right). This finding could have been predicted given that gradient-sensing is an actin-independent process. Like in the case of uniform cAMP stimulation, the immobilization of Gβ-YFP at the anterior, as well as the confined diffusion behavior of the fast fraction disappeared upon F-actin disruption.

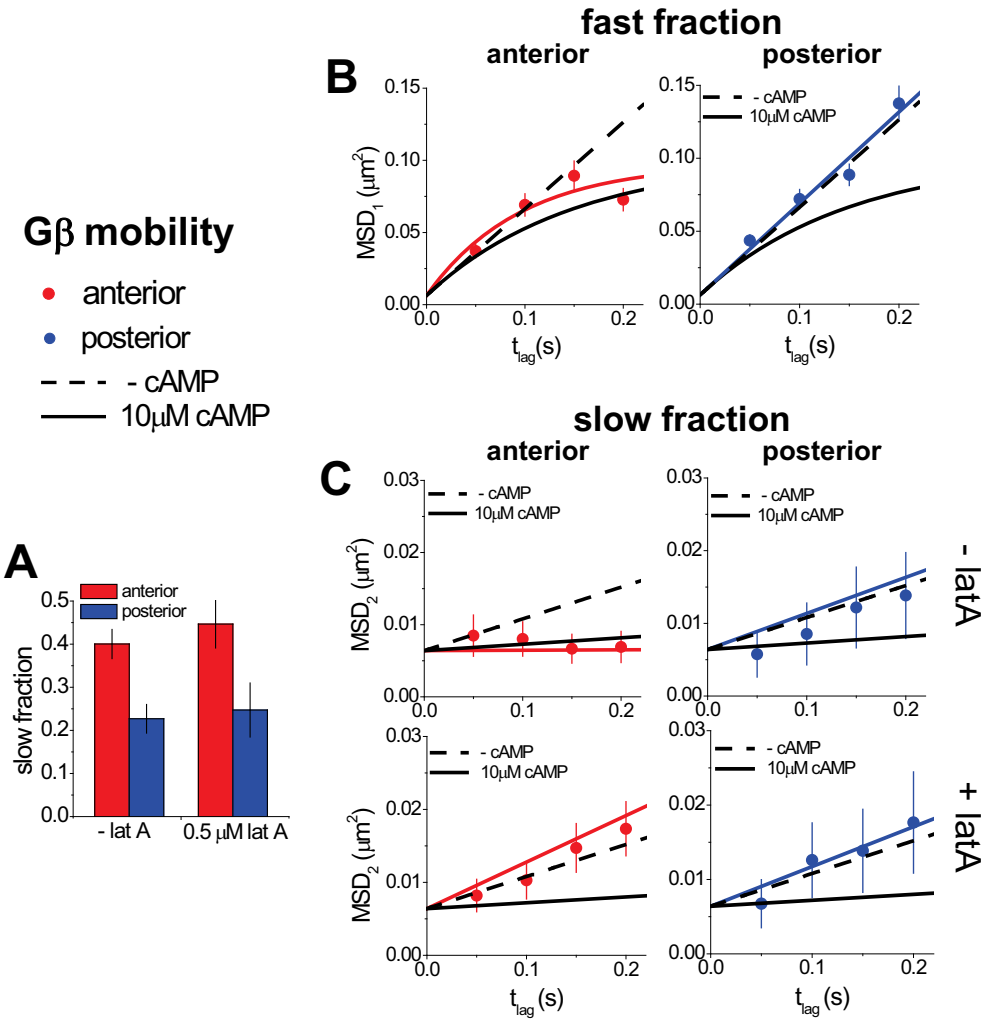
Gβ mobility
anterior
posterior
- cAMP
10μM cAMP
A
anterior
posterior
slow fraction
- lat A
0.5 μM lat A
B
fast fraction
anterior
posterior
- cAMP
10μM cAMP
MSD1 (μm2)
tlag(s)
C
slow fraction
anterior
posterior
- latA
+ latA
MSD2 (μm2)
tlag (s)

Figure 2.5: Gβ-YFP mobility is highly polarized. The diffusion of Gβ-YFP in the anterior (red) and the posterior (blue) apical membrane of wt *D. discoideum* crawling in a shallow (0.4 nM/ μm) cAMP gradient shows distinct differences. The black lines show the results obtained for cells before (dashed line; fig.2.2, left) and after global stimulation with 10 μM cAMP (solid line, fig.2.2, right). **(A)** Slow fraction size of Gβ-YFP in the leading (red) and trailing (blue) edge of wt cells (left) and cells treated with lat A. **(B)** MSD_1 versus time lag for the fast fraction in the leading (red) and trailing edge (blue). Both showed confinement as observed for the fast fraction upon uniform stimulation with cAMP. **(C)** MSD versus time plot for the slow fraction in the leading (red) and trailing edge (blue) in wt cells (left) and cells treated with lat A (right). In the wt cells the slow fraction was immobilized in the front ($D < 0.001$ $\mu m^2/s$). Immobilization was not observed in lat A treated cells.

2.3.7 cAMP-induced domain formation is PI3K and PLA2 independent

To investigate whether the observed cAMP-induced changes in the mobility of the Gβ subunits are the consequence of the activity of the PI3K pathway, we treated the cells with the PI3K inhibitor LY294002. At a concentration of 60 μM and incubation times of 15 min PI3K activity is reduced by > 95% [11]. In the absence of agonist, the inhibitor did not influence the mobility of Gβ subunits. Uniform stimulation with 10 μM cAMP also resulted in diffusion parameters similar to the control situation of wt cells when stimulated with cAMP. The fast fraction was confined, revealing the presence of ∼600 nm domains (fig.2.6C). The slow fraction in LY294002-treated cells was significantly slowed ($D_2 = 0.006 \pm 0.001$ μm^2/s) but mobile (fig.2.6B). As in the control experiments on global cAMP stimulation, the size of the slow fraction grew by 17% (fig.2.6A).

The observed results suggested that the F-actin-dependent domain formation was PI3K activity independent. Although the PI3K/PTEN pathway is known to be important for ligand-induced actin polymerization probably the latter finding is justified by the presence of parallel pathways. Therefore in addition to LY294002 we also used the PLA2 inhibitor bromoenol lactone (BEL) at a saturating concentration of 5 μM [11]. Cells were incubated with both inhibitors and subsequently stimulated with 10 μM cAMP. Treatment with both inhibitors did not result in any significant change in the mobility as compared to treatment with LY294002 alone (fig.2.6B). This result further proved the notion that additional pathways act in parallel to PI3K and PLA2 pathways and that they are sufficient for actin reorganization albeit at a reduced efficient as compared to when all pathways are active.

2.4 Discussion

The spatiotemporal behavior and interaction of activated GPCRs with G proteins constitutes a key event in chemotaxis. Using single-molecule epifluorescence microscopy we measured G protein diffusion in the absence and presence of agonist and in cells in an agonist gradient. By analysis of the mobility in various signaling states we developed a mechanistic model of the early steps in chemotactic signaling (fig.2.7). In the inactive state (fig.2.7, top) G proteins at the membrane are

in either of two fractions, a highly mobile Gα2$\beta\gamma$ heterotrimer or a low-mobility receptor/Gα2$\beta\gamma$ precoupled complex. The receptor/Gα2$\beta\gamma$ complex, which accounts for 32% of the membrane-bound Gα2, 32% of the G$\beta\gamma$, and 50% of the activateable receptor population was identified by comparison of their mobility. Binding of the G protein to the receptor leads to a slow-down in its mobility by one order of magnitude. This latter finding is in line with recent FRAP and TIRM experiments [22] in which an increase in membrane-bound G protein fraction on receptor activation has been found and attributed to G protein / receptor interaction. Given that fast cytosolic proteins [76] are not visible with our technique and only lead to an increased background signal our results provide a detailed view on the membrane-bound fraction and the processes that play a role within the membrane.

Receptor activation by stimulation with cAMP (fig.2.7), bottom) disrupts the equilibrium between the Gα2$\beta\gamma$ heterotrimer and the receptor/Gα2$\beta\gamma$ precoupled complex by allowing the latter to form an activated receptor/Gα2$\beta\gamma$ complex. This intermediate complex subsequently dissociates into a free activated receptor, and into free G$\beta\gamma$ and G$\alpha 2^{GTP}$ subunits. As argued by de Keijzer et al. [17], in turn the activated cAMP-receptor is able to interact with and activate further Gα2$\beta\gamma$ heterotrimers (68% of the initial G$\beta\gamma$ and the membrane-bound Gα2 population) (fig.2.7 bottom, red arrows) resulting in a local increase of G protein activation until cAMP dissociates from cAR1 at a rate of 0.4-1 s^{-1} [45]. It was predicted earlier [17] that such local amplification step, governed by the simultaneous increase in receptor mobility, will lead to a final 5-fold linear amplification of the external cAMP gradient to an intracellular gradient in active G$\beta\gamma$ proteins. The current experiments confirmed this prediction.

In parallel to the increase in fraction size, we observed a slow-down of G$\beta\gamma$ mobility upon stimulation. Since measurements were performed within 20 min after stimulation, a time after which adaptive processes have been initiated [19, 96], we conclude that the immobilization is not transient but persists as long as cells are stimulated. The observation confirms the previously observed dose-dependent steady-state loss-of-FRET which was explained by the dissociation of the Gα2$\beta\gamma$ complex into its subunits [44].

Following G protein activation and further downstream signaling the actin cy-

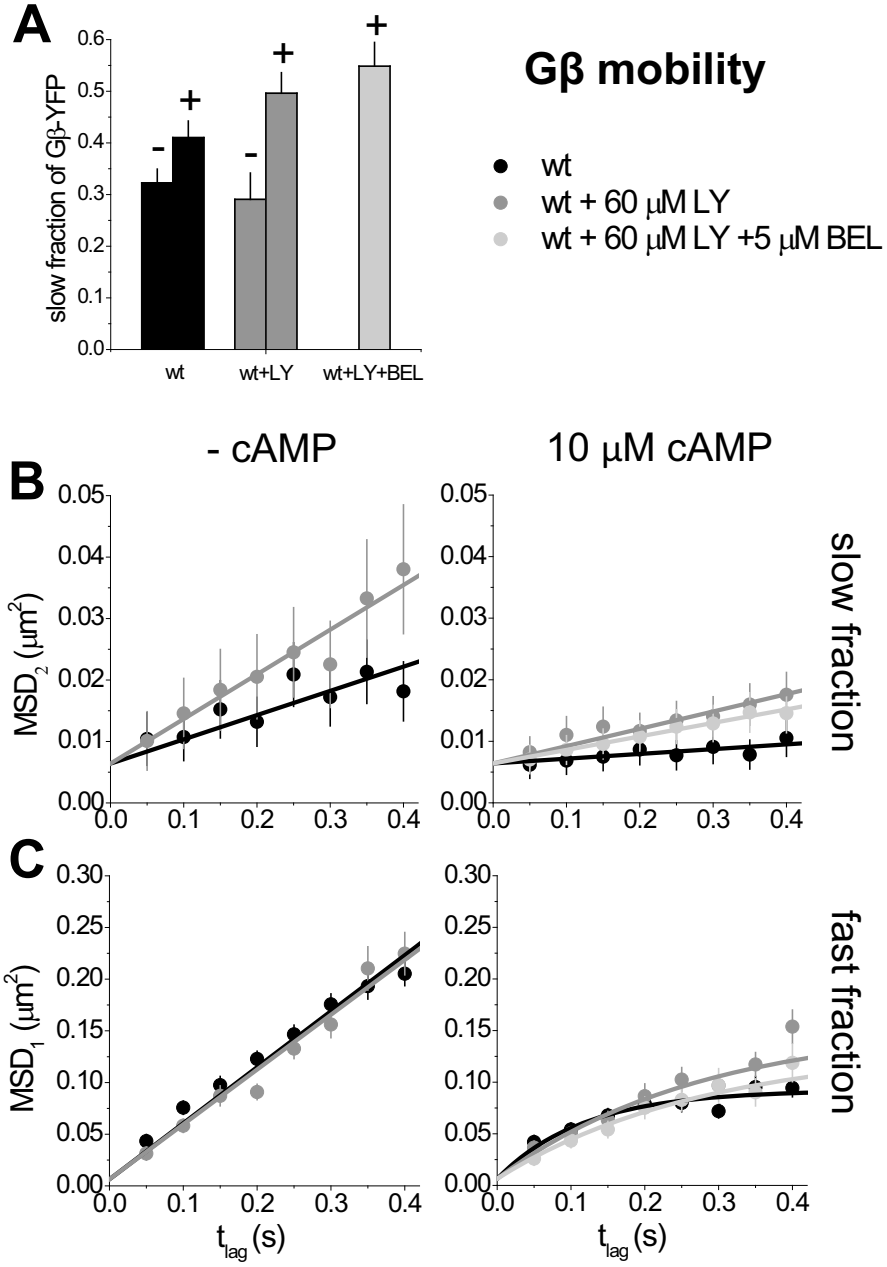
A
slow fraction of Gβ-YFP
0.0
0.1
0.2
0.3
0.4
0.5
0.6
-
+
-
+
+
wt
wt+LY
wt+LY+BEL
Gβ mobility
wt
wt + 60 μM LY
wt + 60 μM LY +5 μM BEL
- cAMP
10 μM cAMP
B
MSD2 (μm2)
0.00
0.01
0.02
0.03
0.04
0.05
0.0
0.1
0.2
0.3
0.4
slow fraction
C
MSD1 (μm2)
0.00
0.05
0.10
0.15
0.20
0.25
0.30
tlag (s)
fast fraction

Figure 2.6: Mobility of Gβ-YFP on inhibition of PI3K and PLA2. Diffusion of Gβ-YFP on the apical membrane of wt *D. discoideum* treated with the PI3K inhibitor LY294002, and the PLA2 inhibitor Bromoenol Lactone (BEL). **(A)** Size of the slow fraction of Gβ-YFP before and after uniform stimulation with 10 µM cAMP in wt cells (black), cells treated with LY294002 (grey), and cells treated with both LY294002 and BEL (light grey). **(B)** MSD_2 versus time lag of the slow fraction of Gβ-YFP in wt cells (black), cells treated with LY204002 (grey), and cells treated with both LY294002 and BEL (light grey) before (left) and after (right) uniform stimulation with 10 µM cAMP. cAMP stimulation caused a dramatic slowdown of the diffusion of the slow fraction in wt cells. This slowdown was impaired after treatment with both inhibitors. **(C)** MSD_2 versus time plot of the fast fraction of Gβ-YFP in wt cells (black), cells treated with LY294002 (grey), and cells treated with both LY294002 and BEL (light grey) before (left) and after (right) uniform stimulation with 10 µM cAMP. Confinement upon cAMP stimulation was observed even in presence of both LY294002 and BEL. These findings suggest that a third parallel pathway, which was not inhibited (most likely the TorC2 pathway [48]) is acting in gradient sensing.

toskeleton is reorganized [27]. Reorganization leads to a tightening of the membrane associated F-actin, apparent in Gα2 and G$\beta\gamma$ mobility which shows confinement to F-actin dependent domains of $\sim$600 nm in size. At this point it is still unclear whether F-actin is sufficient for G$\beta\gamma$ immobilization or whether associated proteins are needed to allow for the immobilization to occur. Inhibition of downstream PI3K (with 60 µM LY294002) and PLA2 (with 5 µM bel-inhibitor) however revealed that the G$\beta\gamma$ slow down was PI3K and PLA2 dependent only to a certain degree. Complete immobilization, as in the control experiment, was not observed. This might indicate either immobilization of only a part of the G$\beta\gamma$ subunits or binding to less rigid F-actin fibers. The formation of the 600 nm F-actin dependent domains, in contrast, was undisturbed. The restriction of activated signaling molecules to a small part of the membrane by inhibiting them from moving across the cell leads to a suggestive biological role for F-actin mediated confinement. Indeed the leading edge of moving fish epidermal keratocytes has been described as a diffusion barrier, even for lipids [94].

Clustering signaling components in a multicomponent signaling complex via a scaffold and/or anchoring proteins to the cytoskeleton was found for various signaling cascades [71] and seems ubiquitous. After initial G protein activation and respective activation of downstream signaling leading to enhanced actin polymerization at the front, activated G$\beta\gamma$ subunits are constrained to actin-dependent scaffolds at the leading edge. This process which spatially restricts G$\beta\gamma$ signaling may in turn lead to a further enhancement of the related signaling cascade at the anterior of the cell in an F-actin dependent positive feedback loop. This process may facilitate chemotactic signaling by spatially restricting the activated signaling components in a larger protein complex; a signalosome. Our data show that, if domains are present before stimulation, they must have a side-length of $L > 1$ µm (fig.2.2C, left). Upon stimulation such domains shrink to $L = 600$ nm (fig.2.2C, right). Assuming a homogeneous distribution of receptors and G proteins in the cell membrane (surface area = 540 µm^2, see section 2.2.8) before stimulation we estimate that such domains on average contain $4 \cdot 10^4$ receptors / 540 µm^2 $\cdot$ (600 nm)^2 = $\sim$27 receptors, $\sim$48 Gα2 subunits and $\sim$52 G$\beta\gamma$ subunits. Experiments performed on F-actin depleted cells have revealed that gradient sensing, the mere detection of the chemical gradient, was

not impaired [70]. Hence, the role of G$\beta\gamma$ immobilization is likely related to the stabilization of pseudopods and perhaps, at a later stage, to the development of an innate cell polarity as is observed after prolonged directional stimulation of *D. discoideum* [27].

A variety of studies have clearly demonstrated that gradient sensing is reflected as a remarkable relocation of signaling components shortly after application of the chemical gradient [70, 15, 100]. Phosphatidylinositol-3,4,5-trisphosphate (PI(3,4,5)P_3) and its related kinase (PI3K) are largely localized at the leading edge whereas their related phosphatase (PTEN) is excluded from the anterior [40]. Despite extensive research relocation of neither the receptor nor the G protein has ever been observed. Protein behavior and activation can be different at different locations due to local variations in membrane curvature [25], activated signaling cascades [90], and the presence of signaling scaffolds [71]. Our experiments here show, as for the cAMP receptor, that cell polarization is reflected in a dynamical property of the G proteins, namely their mobiliy, rather than in their localization. It is noteworthy that the polarized distribution of G$\beta\gamma$ mobility was found to be independent on the presence of F-actin: an identical distribution between fast (inactive) and slow (active) fractions was observed in cells treated with 0.5 µM lat A. Hence, the increase in G protein activity is related to gradient sensing and not to processes responsible for subsequent pseudopod stabilization or amplification and persistent cell polarity.

We and other groups have shown before that polarization in chemotaxing *D. discoideum* cells is present at the level of the GPCR [90, 17]. Here we extended our model and show an F-actin dependent, leading edge specific immobilization of the G$\beta\gamma$ heterodimer, an important mediator of chemotactic responses. We show that this immobilization is due to activation of the chemotactic pathway and hypothesize that F-actin functions either directly or indirectly as a signaling enhancing scaffold, suggesting a function for this mechanism in the stabilization of pseudopods and/or the onset of a persistent leading edge. Likewise, in terms of a balanced inactivation model [59] which suggests a possible inhibitory function for G$\beta\gamma$, binding G$\beta\gamma$ to F-actin would prevent its inhibitory function specifically at the leading edge, finally leading to the steep amplification of the activation signal observed in experiments.

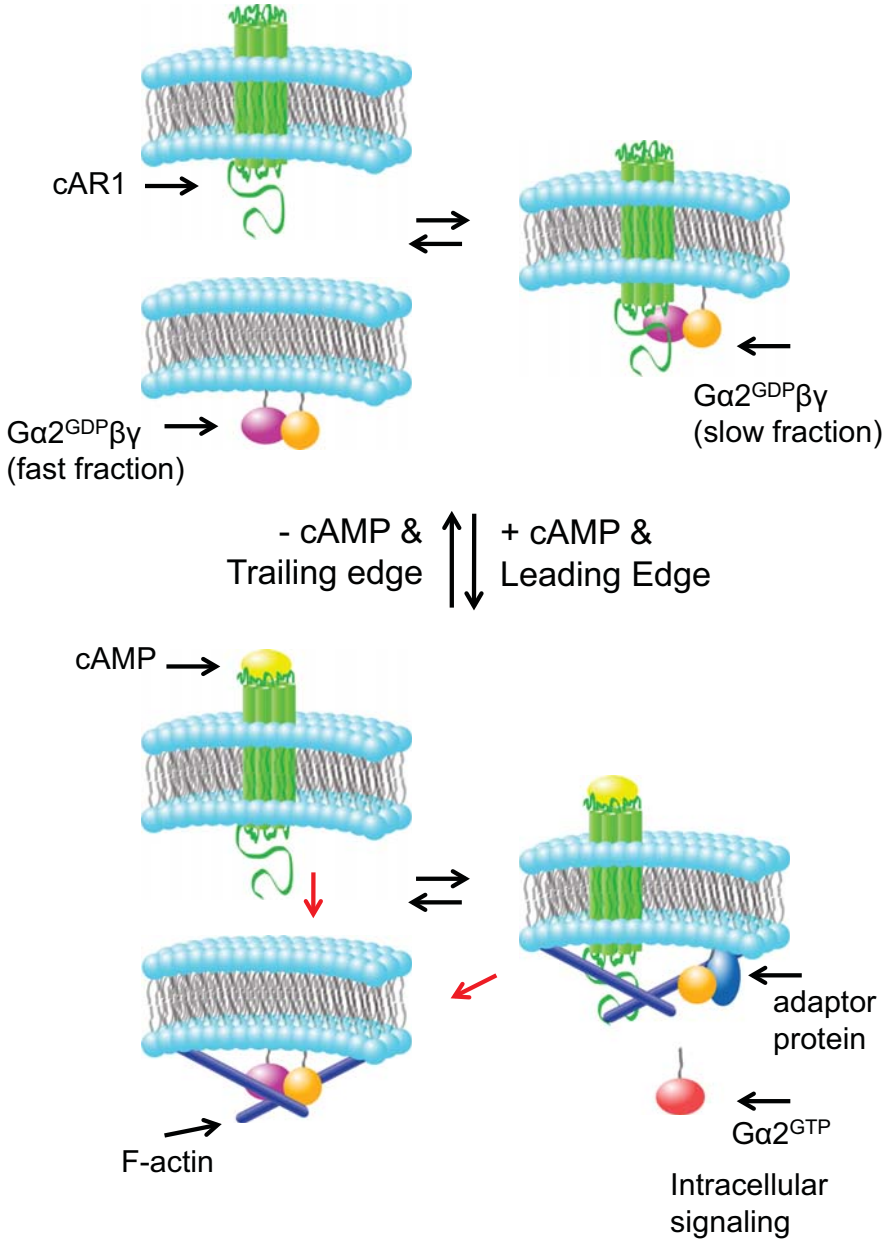
cAR1
Gα2GDPβγ
(fast fraction)
Gα2GDPβγ
(slow fraction)
- cAMP &
Trailing edge
+ cAMP &
Leading Edge
cAMP
F-actin
adaptor
protein
Gα2GTP
Intracellular
signaling

Figure 2.7: Model describing the dynamic cAR1 / G protein interaction at the leading and trailing edge. Before cAMP stimulation (top) the G protein's fast fraction is diffusing freely on the membrane with diffusion constant D = 0.15 $\mu m^2/s$. The slow fraction (D = 0.011 $\mu m^2/s$) exists as a complex which is precoupled to cAR1. 30% of the G protein and about 45% of the receptor population exist in this fraction. Upon binding of cAMP to the receptor (bottom) the G protein heterotrimer is dissociated: the Gα2 subunit exchanges GDP for GTP and diffuses into the cytosol where it is free to activate downstream signaling molecules. The previously precoupled cAR1 fraction is engaged in catalytic activation of the large G protein heterotrimer pool (indicated by red arrows). The G$\beta\gamma$ heterodimeric subunit is immobilized by interaction with F-actin associated structures which potentially serve to locally enhance chemotactic signaling. Tightening of the membrane-associated F-actin restricts the diffusion of the G proteins to $\sim$600 nm domains.

Supplemental information

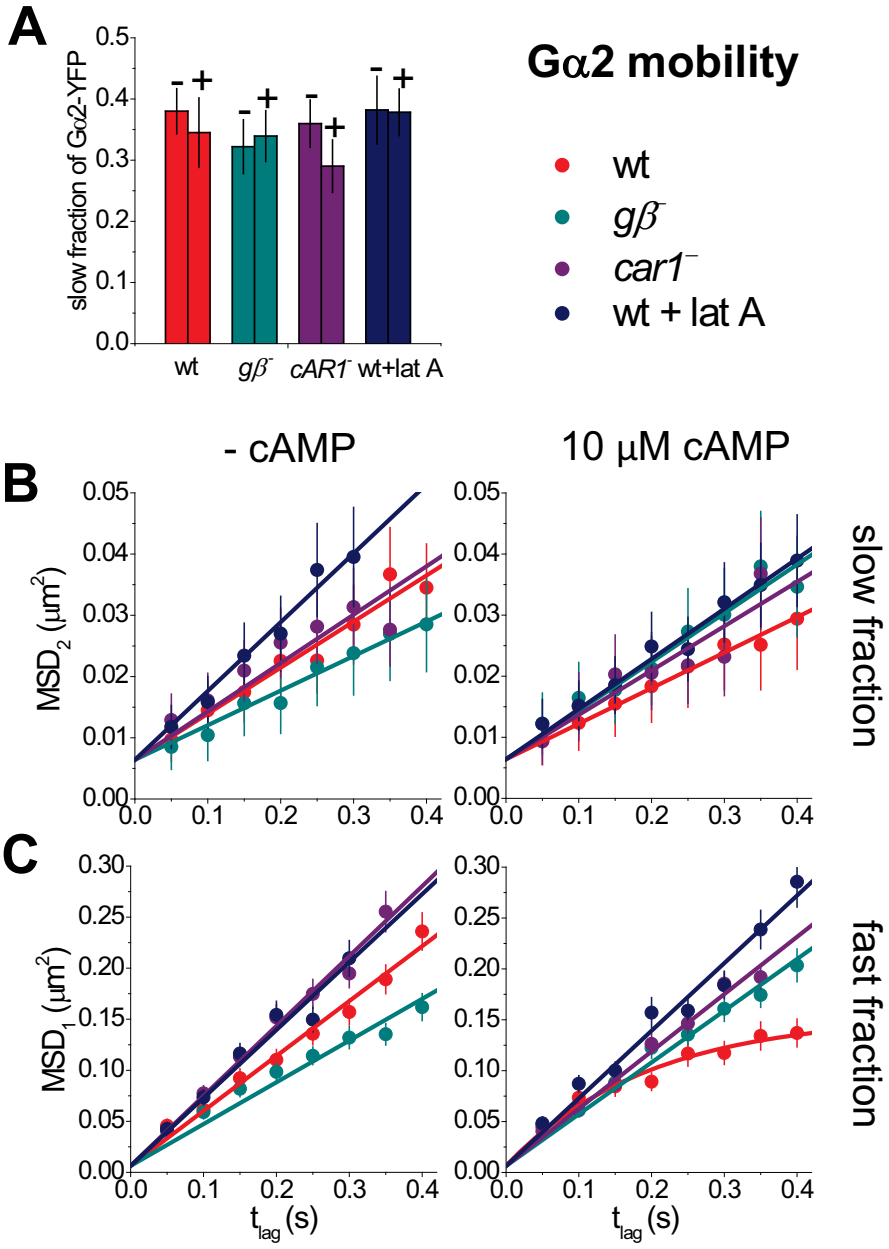

Figure 2.8: Mobility of Gα2-YFP upon stimulation. **(A)** Size of the slow fraction of Gα2-YFP in wt (red), $g\beta^-$ (cyan), *car1*$^-$ (purple), and cells treated with 0.5 µM lat A (blue), before (-) and after (+) global stimulation with 10 µM cAMP. **(B)** MSD_2 versus time lag of the slow fraction of Gα2-YFP in wt (red), $g\alpha2^-$ (cyan), *car1*$^-$ (purple), and cells treated with 0.5 µM lat A (blue) before (left) and after (right) uniform stimulation with 10 µM cAMP. The diffusion of the slow fraction of Gα2-YFP was not influenced by stimulation with cAMP, knockout of $g\beta$, or disruption of the F-actin cytoskeleton. **(C)** MSD_1 versus time lag of the fast fraction of Gα2-YFP in wt (red), $g\beta^-$ (cyan), *car1*$^-$ (purple), and cells treated with 0.5 µM lat A (blue) before (left) and after (right) uniform stimulation with 10 µM cAMP. The diffusion behavior of Gα2-YFP in wt changed from free (eq.2.3) to confined (eq.2.4) upon cAMP stimulation. This was not observed for lat A treated, $g\beta^-$ nor *car1*$^-$ cells.

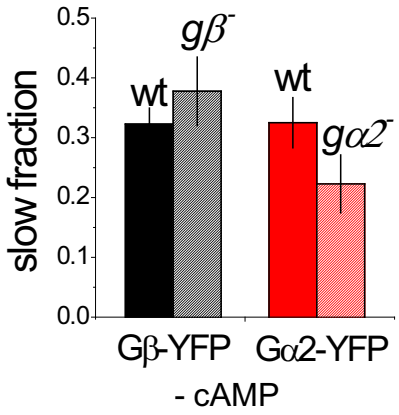

Figure 2.9: Comparison of slow fraction sizes between wt and knockout backgrounds. The slow fraction size of Gβ-YFP in non-stimulated wt and $g\beta^-$ cells (left) is compared to the fraction size of Gα2-YFP in non-stimulated wt and $g\alpha2^-$ cells (right). Both the wt cells and the respective knock-out cells showed a similar size of the slow fraction, assuring that the predominant fast fraction was not an artifact caused by the overexpression of the constructs in wt background.